Simulation of a Birdstrike Impact on Aircraft Canopy Material

T. V. Baughn*
Southern Methodist University, Dallas, Texas
and
L. W. Graham†
General Dynamics, Fort Worth, Texas

The simulation of a birdstrike on a material used in aircraft canopies is performed using the ABAQUS finite-element code. The results of the simulation are compared to the response of a test coupon struck by a rubber ball with properties that provide a load on the coupon comparable to a bird. The displacement-time history of the test coupon is recorded using a high-speed camera. The results of the impact test are compared to the finite-element results. One of the major tasks in developing the simulation was obtaining a load history to apply to the model. The impact load associated with a birdstrike is hydrodynamic, time dependent, and decreases exponentially from the centerline of the impact region. The velocity of impact indicates that material properties at high-strain rates would be required for the simulation. Published material properties at lower strain rates provided adequate information to demonstrate good correlation for the loads examined. Good correlation was achieved in comparing the centerline deflection time histories recorded in the impact test and obtained from the finite-element simulation.

Introduction

THE probability of a birdstrike increases as the number of military aircraft missions requiring high-speed flight at low altitude increases. From March 1976 to March 1986, 2721 U.S. Air Force aircraft had birdstrikes on their canopies (transparencies), of which 109 penetrated into the cockpit. This alarming number of birdstrikes has prompted the aircraft industry to emphasize the "birdproofing" of military aircraft.

In the recent past, the method of birdproofing an airplane was to build and test, then redesign. The capability to predict the response of a transparency to a birdstrike did not exist. The build and test procedure is cost eflective only in aircraft with flat panel transparencies such as airliners. However, as transparencies became highly curved and bubble shaped, as in fighters, this design procedure became very expensive due to the high tooling cost associated with each prototype.

The high cost of prototypes used for birdproofing has promoted the need to examine analytical methods. Finite-element codes (FEC) can be used to represent the complex geometry of the transparency as well as the transient loading of a bird impact. The FEC must also be capable of accounting for geometric nonlinearities (large deflections) and nonlinear material properties of the transparency. Also, depending on bird velocity and weight, large element strains may be present. Until the mid-1970's, there were no known FEC that could handle these difficulties.

Today, several FECs can accommodate material and geometric nonlinearities. A special purpose code called MAGNA (material and geometry nonlinear analysis) developed at the University of Dayton Research Institute was written specifically to handle birdstrike simulations. However, it is the purpose of this work to demonstrate that a commercially available general purpose FEC can simulate a birdstrike. ABAQUS was selected as the finite-element code to simulate the loading and response of the aircraft canopy.

The work presented includes impact testing of a coupon made of the same polycarbonate material as the aircraft canopy. The ball used to impact the coupon has a specific gravity on the same order of magnitude as a bird. The test results were used to generate displacement data for comparison with the finite-element simulation, and also to determine the duration of impact and size of the region of impact on the coupon.

Air Cannon Impact Test

An air cannon impact test is used to test the impact toughness of potential aircraft canopy materials. The air cannon impact test is economical to perform and realistic in that it simulates the loading produced by a birdstrike. A rubber ball is propelled by compressed air into a polycarbonate coupon. The coupon is $25.5 \times 3 \times 0.5$ in. and rigidly clamped on both ends. A high-speed camera running at 5385 frames/s is mounted above the coupon. By analyzing the camera film frame by frame, the displacement-time history of the coupon may be obtained. The simple geometry of the coupon provides for easy comparison between analytical work and actual test results.

The test facility is shown in Fig. 1, which illustrates the support mechanism for the test coupon camera location, and the major components used to propel the rubber ball and measure its velocity. The projectile is bonded to a styrofoam wad and placed in the barrel. The reservoir tank is pressurized to a maximum pressure of 90 psi. The valve is opened and the rubber ball exits the barrel and passes through a light trap that measures its velocity. Five coupons were tested at the maximum pressure, and the projectile velocities ranged from 850 to 825 ft/s. The data reported and compared to the finite-element results were collected at a projectile speed of 835 ft/s since the camera data was clearest at this velocity.

The birdstrike requirement for a typical fighter aircraft transparency is an impact with a 4 lb bird at 350 knots (590 ft/s). Previous birdstrike tests at these conditions have shown no large plastic straining but have shown large displacements and rotations in the material. One of the objectives of the experimental procedure included determining the specific gravity of the rubber ball used to impact the test coupon. The weight and velocity of the projectile must be selected such that the coupon will experience large deformations and rotations in the material but not include large plastic strains as observed in actual birdstrike tests.

Received Feb. 26, 1987; revision received July 15, 1987.

*Associate Professor, Civil/Mechanical Engineering Department.
†Mechanical Engineer, Escape Systems Design.

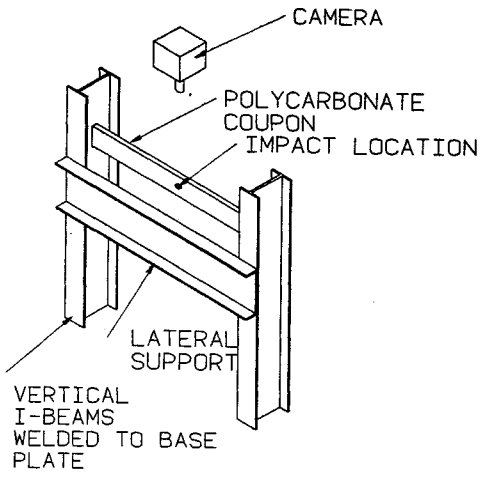

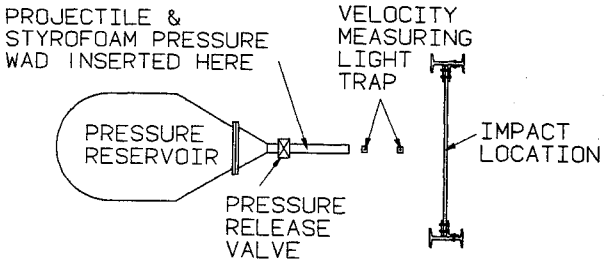

Fig. 1 Air cannon impact tester.

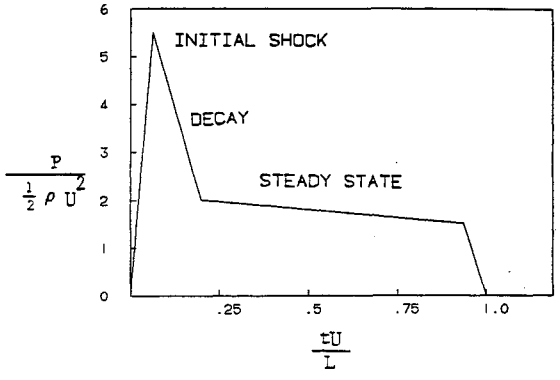

Fig. 2 Impulse load profile at point of impact

The density of the rubber ball has a large influence on the response of the coupon. If a very low density rubber (specific gravity $\ll 1$) is used, insufficient impact energy is generated to simulate a birdstrike. By using a low density ($1 <$ specific gravity < 2) rubber ball, a low strain, large displacement with high material rotation test can be simulated. By using a high density composite rubber ball (specific gravity > 2), large strains may also be induced. These results indicate that the ball should have a specific gravity between 1 and 2.

Hydrodynamic Loading

In solid materials, Wilbeck[1] lists five regions of impact mechanics. These regions are: elastic, plastic, hydrodynamic, sonic velocity, and explosive. The impact regime best suited to describe a birdstrike impact is the hydrodynamic region. In this regime the yield stress of the projectile is greatly exceeded due to its rapid deceleration and may be treated as a fluid. The major factors influencing the impact are the velocity and density. In experimental studies by Barber et al.,[2] the densities of birds of various sizes were measured and found to be 0.549 ± 0.012 oz/in.[3] Since water has a density of 0.578 oz/in.,[3] birds have a specific gravity of approximately 0.95. It is assumed that the bird behaves as a water jet and that the nonisotropic properties of the bird do not greatly influence the results. High-speed camera film shows that a real bird does flow over the target just as a water jet does. For the birdstrike simulation, the projectile will be treated as a perfect fluid with zero shear strength and the target will be treated as elastic and plastic in representing the material properties.

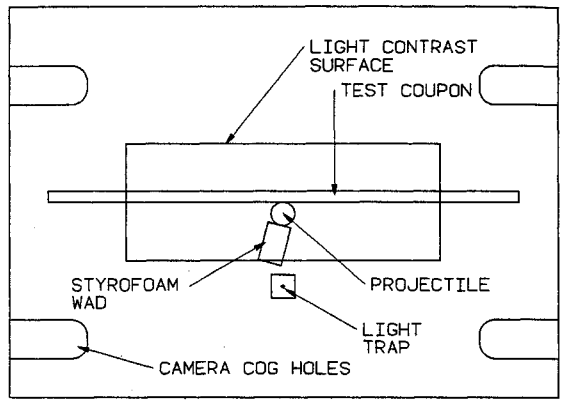

Fig. 3 Schematic to describe the camera records.

The bird must be replaced with an artificial target material when using the air cannon. A replacement material is desirable for convenience and in order to establish test uniformity. Two materials currently used by researchers for this purpose are gelatin and rubber. Since one of the reasons for using an artificial target is convenience, gelatin was omitted.

In a study, Wilbeck tested the impulse loading(s) for low-modulus materials with specific gravities varying from 0.64 to 1.44. In hydrodynamic loading the three load stages are initial shock, pressure decay, and steady state. These three stages are illustrated in Fig. 2 and are typical for a material with a specific gravity of 1.44. In Fig. 2 a nondimensional pressure is plotted vs a nondimensional time where U is velocity, t is time, ρ is density, L is a characteristic length, and P is pressure. Wilbeck found that the peak pressure for all of the artificial materials that behaved similar to a bird were about the same, but that the higher specific-gravity materials showed a higher steady-state pressure. In order to insure adequate loading, a Pr-1750 rubber was selected as the projectile even though its specific gravity is higher than that of a bird. The Pr-1750 rubber is a resilient two-part compound and has a specific gravity of 1.6. The higher specific gravity is needed since the diameter of the rubber ball is limited to 1.25 in., which limits the total weight of the projectile.

During impact, a bird, gelatin, and low specific-gravity rubber all disintegrated and flowed over the target. The Pr-1750, however, did not flow over the target but rebounded back into a sphere. Upon impact the rubber showed incredible elasticity by deforming from a 1.25 in.-diam sphere into a flat sheet of 0.15 in. thickness by 3.5 in. in diameter, then rebounding into its initial shape as seen in Fig. 3–6. Figure 3 is used to describe the photograph shown in Fig. 4–6. The photographs were made from the high-speed camera records.

Load Magnitudes

The pressure in the shocked region can be represented by the water hammer equation for subsonic velocities:

$$P = \rho C_o U_o \tag{1}$$

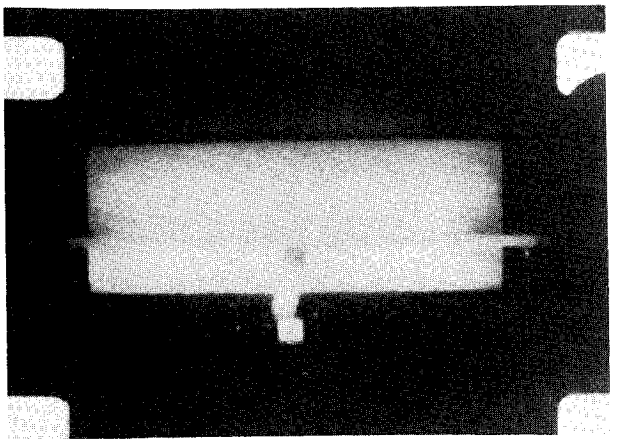

Fig. 4 Projectile at initial impact (time after impact 0.000 s).

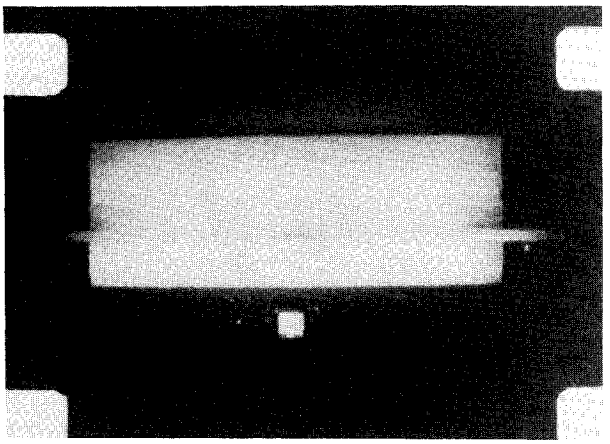

Fig. 5 Projectile in contact and nearly flat on the coupon (time after impact 0.00018 s).

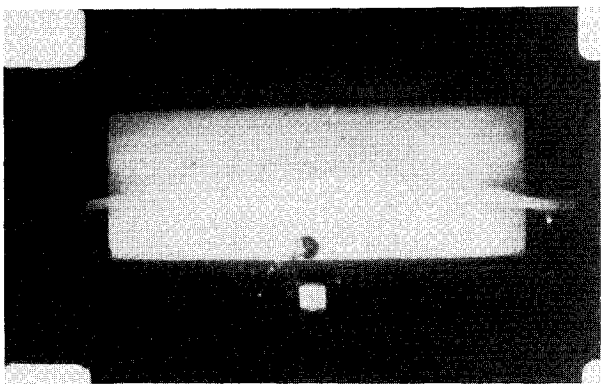

Fig. 6 Projectile rebounding from coupon (time after impact 0.0037 s).

where C_o is the wave velocity in the uncompressed material, and U_o the velocity of the projectile. As the impact velocity approaches higher (supersonic) velocities, the water hammer equation was found to be in error. A modified version of the water hammer equation by Kinslow[3] is the Hugoniot pressure equation:

$$P = \rho U_s U_o \tag{2}$$

where C_o in Eq. (1) is replaced with shock wave velocity U_s. The shock wave velocity is the velocity of the wave traveling from the impacted side of the projectile to the unimpacted side and can be several times higher than the original wave velocity C_o. The increased wave velocity is due to the increased density

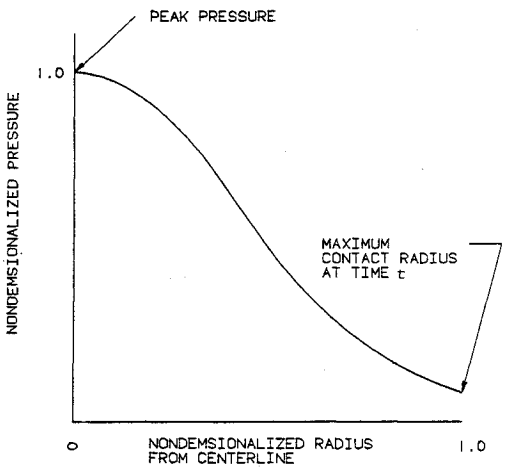

Fig. 7 Radial distribution of steady-state pressure.

Table 1 Material properties and initial velocities for the projectile and target

	Projectile	Target
C_o, ft/s	9137	8438
s[a]	1.419	1.536
ρ, lb_m/ft^3	105.4	74.9
U_o, ft/s	835	0

[a]Reported in Ref. 3.

in the shocked or compressed region. The shock wave velocity is a function of the original density, the shocked density, and the velocity of the projectile. The above equations approximate the peak shock pressure. No equation could be found to represent the pressure in the steady-state stage, but experimental studies have shown it to be 10–30% of the peak pressure.

Equations (1) and (2) are for a rigid target. Testing has shown that rigid targets produce high load magnitudes, but with a shorter impact duration when compared to compliant targets. An aircraft canopy is a compliant target. The compliant target absorbs energy in the form of kinetic energy, plastic deformation, and elastic-strain energy.

Explicit impact loads in compliant targets are very difficult to calculate since they are a function of the target's instantaneous displacement. However, Wilbeck developed the following equation to approximate the compliant effects:

$$P_c = \rho_P U_{SP} U_o \left[\frac{\rho_T U_{ST}}{\rho_P U_{SP} + \rho_T U_{ST}} \right] \tag{3}$$

Equation (3) represents the pressure P_c at the centerline of the projectile target interface. In Eq. (3) the subscripts P and T represent the projectile and target, respectively. The shock wave velocities U_{SP} and U_{ST} for the projectile and target can be calculated from the Hugoniot linear intercept equation reported by Kinslow in Ref. 3, namely

$$U_S = sU_o + C_o \tag{4}$$

where C_o and s are material constants. Material properties and initial velocities for the projectile and target materials are reported in Table 1.

Using the material properties in Table 1 and Eqs. (3) and (4), the centerline pressure P_c was found to be 72,097 psi. This pressure represents the peak shock pressure. The steady-state pressure is assumed to be 10% of the peak pressure. West[4] concluded that a square pulse load showed good agreement between MAGNA and air cannon tests on aluminum plates.

He reasoned that simulating the pressure similar to the loading shown in Fig. 2 resulted in excessive localized deformations. Therefore, the loading to the finite-element model did not include the initial shock pressure as shown in Fig. 2, but did include the steady-state region. The steady-state pressure at the point of impact, which is referred to as the centerline pressure P_c, was held constant at 7210 psi throughout the loading of the model. However, as the ball deformed, the loading away from the centerline changed with time and distance from the point of impact.

The pressure decreases as the distance from the centerline increases. Both Wilbeck[1] and Peterson[5] developed independently the radial pressure distribution by shooting projectiles into an instrumented rigid plate with pressure transducers mounted flush at varying distances from the centerline of the impact point. Both studies concluded that the radial pressure distribution, in the steady-state stage, varied as seen in Fig. 7. The radial pressure distribution P_r can be represented by

$$P_r = P_c e^{-Kr/R(t)} \tag{5}$$

where P_c is the centerline pressure calculated from Eq. (3), K is a constant, r is the radius from the centerline of impact to a load point, and $R(t)$ is the maximum contact radius at time t.

The maximum projectile contact radius $R(t)$ in contact with the target is a function of time and was determined from the air cannon tests by viewing the high-speed camera data. Since $R(t)$ changes with each time step in the transient solution sequence in ABAQUS, the loading distribution on the finite-element model changes with time. The constant K was chosen to be 6.4 in order to meet the boundary condition of insignificant pressure at the maximum radius.

A side view of the test coupon is illustrated in Fig. 8 along with a close-up view of the finite-element model representing one-fourth of the test coupon. The test coupon was modeled with solid elements and the surface has 9 points per element where a load can be applied. A program external to ABAQUS was written to determine the value of P_r for all load points inside the contact area. The program calculates the individual loads for each point using Eq. (5). These calculated loads are updated at each time step and input into ABAQUS.

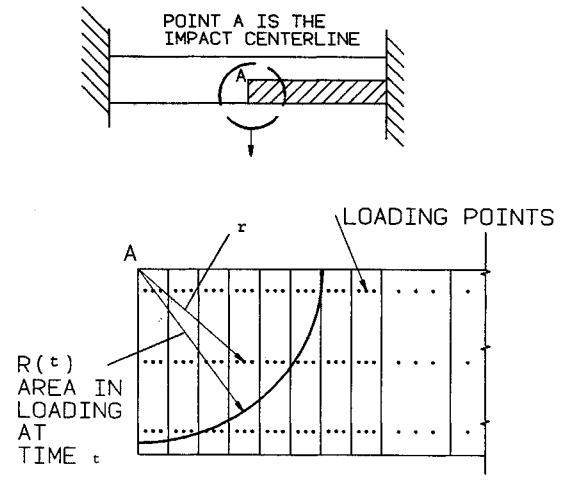

Fig. 8 Illustration of the load points for the finite-element model.

Material Properties

Polycarbonate is a common material used in many aircraft transparencies. Analytical estimates indicate that stress-strain relationships are needed at strain rates of 200–400 in./in./s to model a bird impact. Polycarbonate is difficult to test at these strain rates. Adhesives that are compatible with polycarbonate are gummy and not strong enough to hold an accelerometer or rigid enough for a strain gage. A suitable adhesive for attaching a strain gage will attack the polycarbonate and cause brittleness.

Material properties for polycarbonate have been published by the U.S. Air Force, Materials Laboratory, and Flight Dynamics Laboratory. The study by Hassard[6] tested at strain rates from 0.05 to 20 in./in./min. He reported that as the strain rate increased, the yield strength increases and the elastic modulus almost doubled. A second study by Greene[7] reported material properties at strain rates of 0.025 in./in./min to 200 in./in./s. The elastic modulus reported by Greene was the same as Hassard's at the low strain rates, however, as the strain rate increased the modulus only increased by 10%. Numerical values for the highest strain rates are reported in Table 2.

Since Greene tested at the higher strain rates, his data will be used for the initial simulation calculations and will be treated as elastic perfectly plastic. Yielding was predicted using the Mises-Hencky criterion. After completing the initial simulation with Greene's data, a simulation was conducted using only the elastic material properties reported by Hassard.

Finite-Element Model

The finite-element model of the test coupon is rectangular and only one-fourth of the coupon is represented due to symmetry. The model consists of 21 solid isoparametric brick elements. Each brick element contains 27 nodes. A sketch of the model is shown in Fig. 9. The end of the model away from the impact load is rigidly clamped.

Early in the development of the birdstrike simulation it was thought that the analysis would require the following capability: large displacements, large rotations, large strains, and nonlinear material properties. These capabilities represent the most general load case and computationally the most complex and most expensive. Although ABAQUS is capable of analyzing materials subjected to the above nonlinearities, simulation of

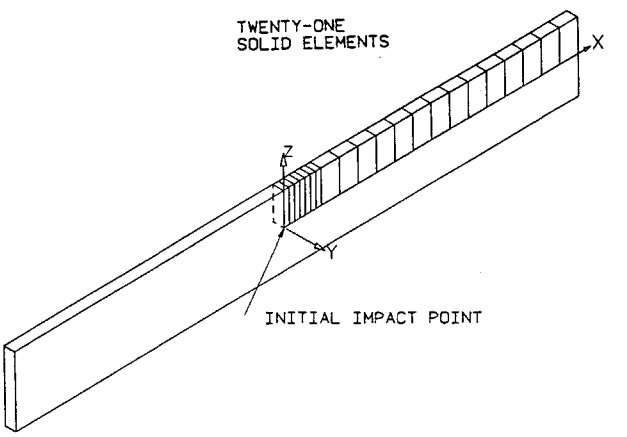

Fig. 9 ABAQUS finite-element model.

Table 2 Material properties for polycarbonate used in the ABAQUS model[a]

Source	Yield stress	Elastic modulus	Plastic modulus	Ultimate stress
Hassard[6]	11.1×10^3	6.56×10^5	—	—
Greene[7]	9.62×10^3	3.39×10^5	6.79×10^3	1.36×10^4

[a]Modulus and stress values are reported in psi.

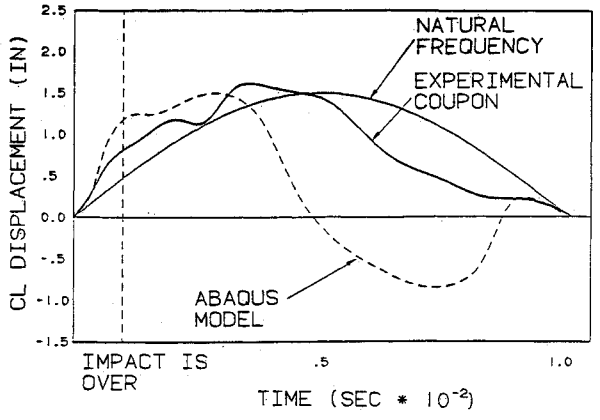

Fig. 10 ABAQUS simulation with fixed end constraints.

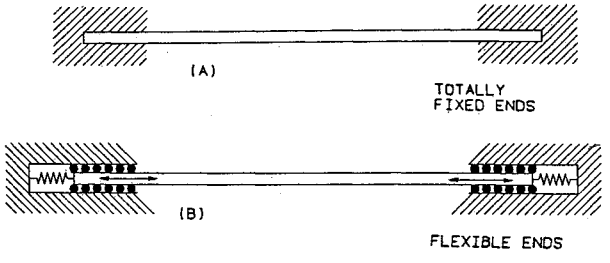

Fig. 11 Original end constraints (A) and modified end constraints (B).

the birdstrike showed that the large-strains capability was not needed and material nonlinearity was found only in the impact area. ABAQUS utilizes the updated Lagrangian approach for a nonlinear solution sequence.[8] A local coordinate system is attached to each element and moves with the element, sharing its rigid body motion. All strains and stresses are calculated and reported in the local coordinate system for each element.

Success Criteria

The success of the birdstrike simulation depends upon agreement between the displacement time history and displacement frequency for both the finite-element model and the experimental impact data. The displacement frequency is defined as the frequency at which the center of the coupon oscillates about the longitudinal axis due to the impact load. Before running the impact simulation a comparison of the natural frequencies of the finite-element model, classical beam theory, and a modal test of the experimental coupon was conducted. All three results agreed upon a first natural frequency of 43 ± 1 Hz. These results imply that the finite-element model is a good representation of the experimental coupon.

Initial Simulation Attempt

The camera data from the experimental test showed that the impact load was applied for 0.0012 s which is approximately one-twentieth of the period of the first natural frequency of the coupon. In the finite-element simulation the load was removed after 0.0012 s and the simulation was a free vibrational problem. The load was applied as described in the hydrodynamic loading section. Greene's data was used for material properties.

The simulation was stopped at 0.0058 s, which corresponds to a one-quarter cycle and maximum deflections. The comparison of the displacement time history of the center point of the coupon showed that the ABAQUS model underestimated the displacement of the test coupon. The model was run again with

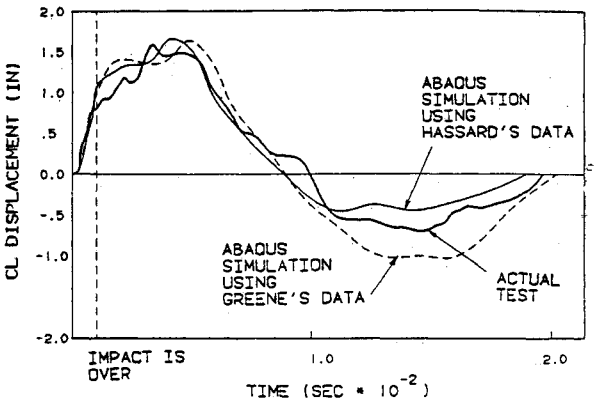

Fig. 12 ABAQUS simulation with modified end constraints.

an upward adjustment in the pressure loading and another comparison was made. This process was repeated until the maximum deflection of the finite-element model agreed with the maximum deflection of the experimental coupon. The centerline pressure necessary for these deflections to match was 12,750 psi as compared to the initial pressure of 7210 psi. The displacement-time histories showed reasonable agreement for the first 0.004 s. The computer simulation was then allowed to continue for an additional one-quarter cycle, or to 0.0116 s. The results are shown in Fig. 10. After the maximum deflection was reached (0.004 s) the model displacement time history deviated significantly from the experimental results. In addition, the frequency of the experimental coupon was 43 Hz, which corresponds to the first natural frequency where the ABAQUS impact load results imply a higher frequency of 88 Hz. These results did not meet the success criteria.

Model Modifications

Several modifications were made to the ABAQUS model in order to improve the correlation with the experimental data. The modifications were associated with 1) the model element density (number of elements per inch), and 2) model end conditions. Increasing the element density did not significantly affect the ABAQUS displacement frequency, but altering the model end conditions did significantly influence the results.

The original finite-element model was assumed to have fixed end constraints. The experimental coupon was bolted and clamped in a steel holding fixture during impact. Since the modulus of the steel fixture is much greater than the modulus of the plastic coupon, the assumption was made initially that the holding fixture was infinitely rigid during bending of the specimen. Later, it was observed that the impact loads not only put the specimen in bending but also in tension. Therefore, the tensile stiffness of the experimental fixture was determined and used to accurately simulate the fixture end conditions in the ABAQUS model. The stiffness was experimentally determined by pulling on the fixture with a known load and measuring the extension of the fixture. Based upon this measurement, a modified end condition for the ABAQUS model is shown in Fig. 11 with the spring constant of 1130 lb/in. The initial end constraint is also illustrated.

Upon running the ABAQUS model with the remodeled end conditions, the ABAQUS displacement frequency and the experimental displacement frequency agreed. The added flexibility of the model caused an increase in deflection in the ABAQUS results. Once again, a trial and error process was used to obtain the correct maximum deflection resulting in a centerline pressure load of 9350 psi, which is much closer in agreement to the calculated pressure of 7210 psi.

The ABAQUS centerline displacement-time history is shown in Fig. 12 for material properties reported by Greene and Hassard. After half a cycle, the simulation overestimated the

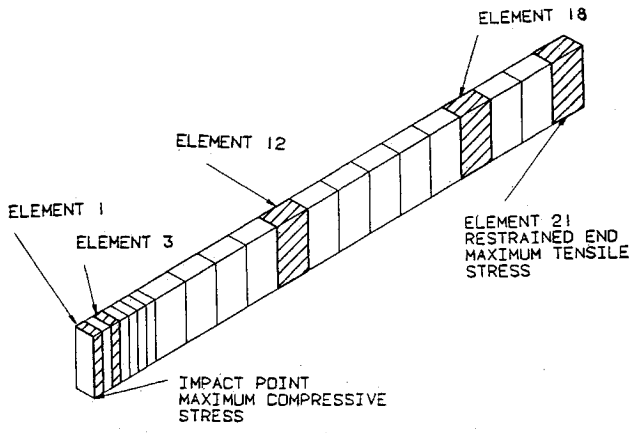

Fig. 13 Location of elements corresponding to coupon failure locations.

deflection using Greene's data and underestimated the deflection using Hassard's data. Throughout most of the cycle, however, the simulation and experimental results agree.

In addition to the centerline displacement time history agreement between the ABAQUS model and the experimental coupon, a comparison was also made between the experimental and simulated results at various other points along the coupon. For these other points, the results from the ABAQUS model also agreed with the results from the experimental coupon. Although the selection of material properties influenced the results, the prediction capability of the model has been verified. The ABAQUS model with the modified end constraints meet the success criteria.

Element Stresses and Strains

The largest first principal stress (tensile) occurred in the ABAQUS model near the end restraints and has a magnitude of +13,000 psi with Hassard's data and +11,500 psi using Greene's data. Although the stress magnitudes are large relative to the ultimate stress reported by Greene in Table 2, the duration is very short. Using Greene's data, the largest elastic and plastic strains were 3 and 0.5%, respectively, and both occurred at the impact point. A dimensional check of the experimental coupon after the impact indicated very little permanent set except in the impact region. This implies that there was very little plastic strain outside the impact region and agrees with the above ABAQUS results. With Hassard's data, the largest elastic strain was 2%. No plastic strains were calculated since total elasticity was assumed in the ABAQUS model using Hassard's material properties.

During testing it was noted that about 10% of the air cannon impact tests resulted in failure of the coupon, usually due to substandard polycarbonate. Most of the failures originated on the loaded side of the coupon at a location that corresponds to elements 12 and 18 as shown in Fig. 13. The maximum tensile stresses in elements 12 and 18 were in the 9–10,000 psi range. Although other elements see very high stresses, elements 12 and 18 are the first elements to see significant stresses. Therefore, ABAQUS is correctly predicting the failure location if the polycarbonate is substandard.

Summary

Good correlation was achieved between the actual test and the ABAQUS simulation using either Greene's or Hassard's material data. The simulation clearly identifies the method of restraint as a key parameter in obtaining satisfactory results. For the impact loads examined there was little plastic deformation and large strain capability was not needed. If higher velocity impacts are to be studied, then a more extensive material data base will be required to represent the material properties at higher strain rates and potentially large strains. A good estimate of the impact load can be obtained using the compliant target formulation and the water hammer equation.

References

[1]Wilbeck, J. S., "Impact Behavior of Low Strength Projectiles," Air Force Materials Lab. Rept. AFML-TR-77-134, July 1978.

[2]Barber, J. P., Taylor, H. R., and Wilbeck, J. S., "Bird Impact Forces and Pressures on Rigid and Compliant Targets," Air Force Flight Dynamics Lab. Rept. AFFDL-TR-77-60, May 1978, p. 24.

[3]Kinslow, R., *High-Velocity Impact Phenomena*, Academic, Inc. 1970, pp. 294–372.

[4]West, B., and Brockman, R. A., "Evaluation of Bird Load Models for Dynamic Analysis of Aircraft Transparencies," Air Force Flight Dynamics Lab. Rept. AFFDL-TR-80-3092, Aug. 1980, pp. 30–36.

[5]Peterson, R. L., "Bird Impact Forces in Aircraft Windshield Design," Air Force Flight Dynamics Lab. Rept. AFFDL-TR-75-150, March 1976, pp. 30–36.

[6]Hassard, R. S., "Design Criteria Transparent Polycarbonate Sheet," Air Force Materials Lab. Rept. TR-72-117, Aug. 1978.

[7]Greene, F. E., "Testing for Mechanical Properties of Monolithic and Laminated Polycarbonate, Part 1 Test Results and Analysis," Air Force Flight Dynamics Lab. Rept. AFFDL-TR-77-96, Oct. 1978.

[8]Hibbitt, Karlson and Sorensen, Inc., *ABAQUS Theory Manual*, Providence, RI, Sept. 1984.